Hybrid Carbon Nanotubes–TiO2 Photoanodes for High Efficiency Dye Sensitized Solar Cells

ARTICLE *in* THE JOURNAL OF PHYSICAL CHEMISTRY C · JULY 2013

Impact Factor: 4.77 · DOI: 10.1021/jp403553t

9 AUTHORS, INCLUDING:

Isabella Concina
Università degli Studi di Brescia
64 PUBLICATIONS **823** CITATIONS
SEE PROFILE

Giorgio Sberveglieri
Università degli Studi di Brescia
580 PUBLICATIONS **12,189** CITATIONS
SEE PROFILE

Federico Rosei
Institut national de la recherche scientifique
278 PUBLICATIONS **5,152** CITATIONS
SEE PROFILE

Alberto Vomiero
Luleå University of Technology
140 PUBLICATIONS **2,748** CITATIONS
SEE PROFILE

THE JOURNAL OF PHYSICAL CHEMISTRY C

Article

pubs.acs.org/JPCC

Hybrid Carbon Nanotubes–TiO_2 Photoanodes for High Efficiency Dye-Sensitized Solar Cells

Kadiatou Therese Dembele,[†,‡,¶] Gurpreet Singh Selopal,[§,∥,¶] Caterina Soldano,[§,∥] Riad Nechache,[†,‡] Julio Cesar Rimada,[⊥] Isabella Concina,*[,§,∥] Giorgio Sberveglieri,[§,∥] Federico Rosei,*[,†,#] and Alberto Vomiero*[,§,∥]

[†]Institut National de la Recherche Scientifique, Énergie, Matériaux et Télécommunications, 1650 boul. Lionel-Boulet, Varennes, Québec J3X 1S2, Canada

[‡]Department of Chemical Sciences and Technology & NAST Center, University of Rome Tor Vergata, Via della Ricerca Scientifica 1, 00133 Rome, Italy

[§]CNR IDASC SENSOR Lab, Via Branze 45, 25123 Brescia, Italy

[∥]Department of Information Engineering, Brescia University, Via Valotti 9, 25133 Brescia, Italy

[⊥]Solar Cells Laboratory, Institute of Materials Science and Technology (IMRE), University of Havana, Zapata y G, Vedado, 10400 La Habana, Cuba

[#]Center for Self-Assembled Chemical Structures, McGill University, 801 Sherbrooke Street West, H3A 2K6 Montréal, Québec, Canada

Supporting Information

ABSTRACT: We describe a fast and effective procedure for the preparation of high efficiency hybrid photoanodes for dye-sensitized solar cells (DSCs), based on nanocrystalline TiO_2 with limited addition of multiwall carbon nanotubes (CNTs). The mixing process between CNTs and TiO_2 nanoparticles is almost instantaneous, which makes it feasible for large-scale fabrication. Enhanced electron lifetime and reduced charge recombination lead to highly increased short circuit current density and overall photoconversion efficiency (from 13.6 mA cm^{-2} to 16.0 mA cm^{-2} and from 7.0% to 9.0%, respectively, considering the bare TiO_2 and the optimum CNTs concentration, which is 0.010 wt %), while the small reduction in open circuit photovoltage does not significantly affect cell performances. This result is remarkable since a standard dye molecule (N719) was used and no chemical treatments of the photoanodes prior to cell fabrication were applied (i.e., soaking in $TiCl_4$ to boost open circuit photovoltage).

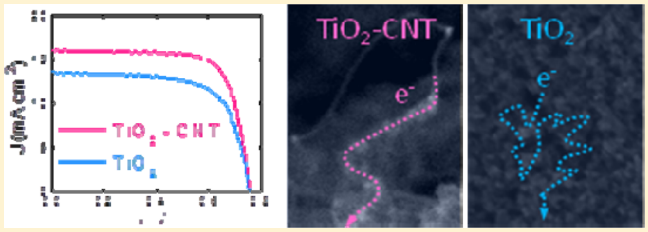

INTRODUCTION

Dye-sensitized solar cells (DSCs)[1,2] are rapidly becoming a promising, realistic, and low-cost alternative to silicon-based solar cells currently in use. Presently, the photoconversion efficiency (PCE) in traditional DSC photoanodes (composed of a thick film made of TiO_2 nanoparticles) is limited by charge transfer to the counter electrode and to charge recombination at the dye or electrolyte interfaces. Recent work on the design of oxide photoanode toward improvement of PCE[3] proposed the exploitation of highly conducting one-dimensional (1D) oxide nanostructures like nanotubes,[4,5] nanowires,[6,7] composite systems,[8,9] or hierarchically assembled photoanodes to address this issue.[10,11] In many cases, the single crystalline nature of the 1D nanostructures assembly has the overall effect of improving electron transport with respect to its polycrystalline counterpart, leading to reduced charge recombination. However, despite great efforts in investigating such alternative solutions, limited results have been obtained in terms of improved functional properties in DSCs.

A potentially appealing alternative to one-dimensional oxide nanostructures is represented by the incorporation of carbon nanotubes (CNTs) in TiO_2 traditional photoanodes.[12−14] CNTs exhibit exceptional physical and chemical properties, which render them outstanding potential candidates for a broad variety of applications ranging from optics to electronics[15] (field-effect transistors (FETs),[16] nanoelectro-mechanical systems (NEMS),[17] sensors,[18] supercapacitors,[19] batteries,[20] etc.).

CNTs, as well as other carbonaceous materials (e.g., graphene,[21,22] graphene oxide,[23] and fullerenes[24]) have been proposed as possible key elements in directing the flow of photogenerated electrons as well as favoring charge injection/extraction in solar cell-based technologies.

Fabrication of hybrid nanostructures comprising a core of multi-walled carbon nanotubes (MWCNTs) surrounded by

Received: April 10, 2013
Revised: June 5, 2013
Published: June 13, 2013

   dx.doi.org/10.1021/jp403553t | J. Phys. Chem. C 2013, 117, 14510−14517

Table 1. Functional Properties of DSCs with Different MWCNT Concentrations

anode structure	CNTs (wt %)	$T_{annealing}$ (°C)	thickness (μm)	PCE (%)	*FF* (%)	V_{oc} (mV)	J_{sc} (mA cm^{-2})	dye loading (mol mm^{-3} × 10^{7})
transparent layer	0	450	12.6	6.5	71.0	745	12.7	1.05
transparent layer	0.003	450	12.5	5.6	68.0	700	11.9	
transparent layer	0.007	450	11.5	6.4	67.1	695	13.8	
transparent layer	0.010	450	12.8	8.1	71.0	724	15.6	1.05
transparent layer	0.015	450	9.9	7.9	71.0	734	15.3	1.65
transparent layer	0.020	450	11.3	7.4	71.0	704	14.8	1.25
transparent layer	0.045	450	8.8	6.7	71.0	698	13.6	1.35
transparent layer	0.075	450	10.1	5.9	73.0	707	11.6	1.35
transparent layer	0.250	450	16.4	1.1	62.0	789	2.2	3.70
transparent + reflecting layers	0	500	15.9	7.0	69.0	755	13.6	
transparent + reflecting layers	0.010	500	16.4	9.0	74.0	758	16.0	

TiO_2 nanoparticles[25] or incorporation MWCNTs (1 wt %) at relatively low temperature processes (150 °C)[26] have been proposed. However, in this case, limited PCE was achieved, likely due to poor sintering due to low-temperature synthesis. CNT-based architectures can be used as a conducting scaffold in a TiO_2 semiconductor based photoelectrochemical cell with the effect of increasing the PCE by a factor of 2 (ref 7) or cell stability.[27]

Here, we present a simple, fast, and low-cost fabrication method for the integration of MWCNTs in TiO_2 photoanodes to enhance the functional properties of DSCs. The process is highly reproducible and leads to 25% improvement of PCE with respect to the photoanode without adding CNTs. Our results demonstrate the occurrence of an upper limit for CNT loading, above which radiation absorption from CNTs and disordered CNT assembly negatively affect the properties of solar cells (short circuit current density (J_{sc}), fill factor (*FF*), and PCE).

EXPERIMENTAL METHODS

Mesoporous TiO_2 films were prepared by tape casting commercial TiO_2 paste composed of 20 nm sized anatase nanoparticles (18 NR-T from Dyesol) onto transparent FTO glass substrates (sheet resistance 10 ohm/square). The thickness of the tape during the casting process was 50 μm. The drying process was followed for 15 min at ambient atmosphere and temperature and then for 6 min at 120 °C. After drying, all the photoanodes were then annealed at 450 °C for 30 min in ambient atmosphere.

An ethanolic suspension of MWCNTs (from Sigma-Aldrich, cat. no. 698849, 10 μm average length) was prepared (0.006 g of MWCNTs in 15 mL of ethanol) and sonicated for 3 h to obtain a good dispersion of MWCNTs in ethanol. A precise amount was then mixed with a known weight of TiO_2 paste, to obtain a mixed composite containing fixed percentages in weight of MWCNTs. The MWCNT−TiO_2 paste was tape casted on FTO glass under the same conditions as described above. All the photoanodes were then annealed at 450 °C for 30 min in ambient atmosphere. The final percentage of CNT incorporated in the TiO_2 photoanode was estimated taking into account the photoanode weight after annealing. The weight loss of TiO_2 paste after annealing was evaluated by gravimetry and found to be 80% of the original wet weight.

XRD analysis was carried out using a Bruker D8 Advance diffractometer equipped with a CuKα X-rays source, λ = 1.542 Å.

Optimized cells were fabricated by tape casting an additional scattering layer of TiO_2 nanoparticles (WER2-O anatase particles from Dyesol, 150−250 nm in size) on top of two different layers: (i) TiO_2 without MWCNTs and (ii) TiO_2 with 0.010% of MWCNTs. In this case, the annealing temperature was increased to 500 °C to improve the sintering process.

The thickness of the photoanodes after calcination was measured using a stylus profilometer and is given in Table 1.

After annealing, the photoanodes were dye-sensitized by immersion into 0.5 mM ethanolic solution of commercial Ru-based complex molecular N719 dye (from Solaronix) for 24 h and then washed with ethanol to remove excess of unabsorbed dye molecules.

Dye loading was quantitatively evaluated by UV−vis spectrophotometry (T80 spectrophotometer, PG Instruments) after complete removal of the dye from the photoanode with 0.1 M aqueous NaOH.

Diffuse reflectance infrared Fourier transform (DRIFT) spectra were collected under vacuum on a Bruker VERTEX70v spectrometer (accumulating 32 scans at a resolution of 4 cm^{-1}) and displayed in the Kubelka−Munk unit.[28,29] A few milligrams of each sample were mixed with KBr and loaded in the accessory for diffuse reflectance (Harrick Scientific); KBr was used as a background.

The DSCs were fabricated by using the I_3^-/I^- redox couple electrolyte, platinized FTO as counterelectrode (5 nm thin film of Pt on FTO by sputtering), with 25 μm thick spacers (from Solaronix) between the photoanode and the Pt counter-electrode. The redox electrolyte was composed of 0.1 M LiI, 0.05 M I_2, 0.6 M 1,2-dimethyl-3-*n*-propylimidazolium iodide, and 0.5 M 4-*tert*-butylpyridine dissolved in acetonitrile. All chemicals were purchased from Sigma−Aldrich and used without any further purification.

The current−voltage (*I*−*V*) characteristics of the fabricated cells were measured by a Keithley 2400 SourceMeter under simulated sunlight using an ABET2000 solar simulator at AM1.5G (100 mW cm^{-2}) calibrated using a reference silicon cell and mechanical filters. During the measurement, the cell was masked with a square mask, and the irradiated area was 0.25 cm^2. The TiO_2 layer, square in shape, has dimensions slightly larger than the mask, for a typical active area of around 0.27−0.30 cm^2. The impedance spectroscopy was carried out in dark conditions of illumination using a SOLARTRON 1260 A Impedance/Gain-Phase Analyzer, with an AC signal of 20 mV in amplitude, in the frequency range between 10 mHz and 300 kHz. The applied bias was between 0 V and 100 mV above the open-circuit voltage of the solar cell.

dx.doi.org/10.1021/jp403553t | J. Phys. Chem. C 2013, 117, 14510−14517

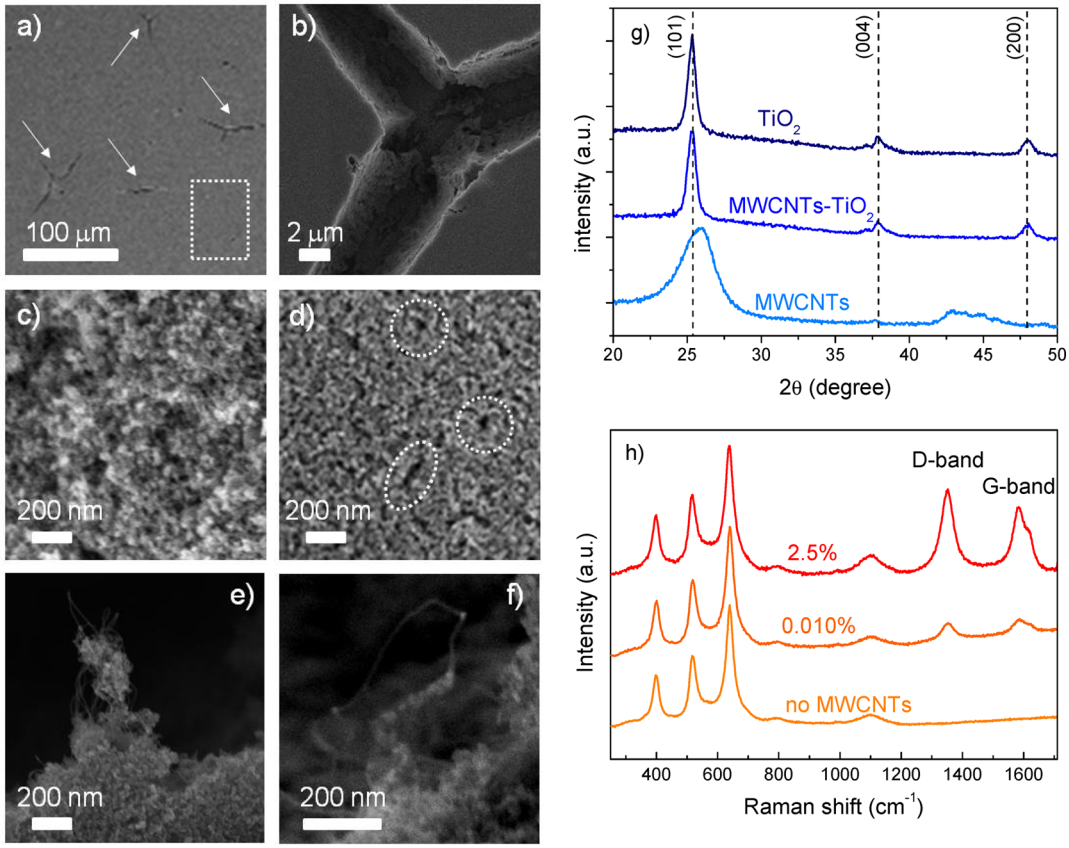

Figure 1. (a,b,d–f) SEM images of the 0.25% sample at various magnifications. Deep cracks induced by the presence of the MWCNTs are clearly visible in panels a (white arrows) and b. The dotted rectangle in panel (a) highlights a crack-free zone, similar to the standard surface morphology recorded for all the other samples. (c) SEM image of bare TiO_2 film. (g) XRD patterns of MWCNTs, bare TiO_2, and 0.25% sample. (h) Raman spectra of bare TiO_2 and 0.010% and 2.5% samples.

RESULTS AND DISCUSSION

Hybrid MWCNT–TiO_2 photoanodes were prepared by dispersing commercial MWCNTs in an ethanol-based solution (see Experimental Section), and then adding precise quantities of such solution (for CNTs concentration ranging from 0.01 to 0.25 wt % in the final composite) to a commercial TiO_2 paste composed of 20 nm sized anatase nanoparticles. Such a mixture is then processed according to the standard preparation procedure (tape casting on fluorine-doped tin oxide (FTO) glass followed by 30 min firing at 450 °C) obtaining film thicknesses in the range 4–20 μm. The concentration of MWCNTs ranged from 0 wt % to 0.250 wt %. The addition of CNTs modifies the optical properties of the TiO_2 layers according to the percentage considered (see Supporting Information, Figure S1). The film transparency in the UV–vis range remains unchanged for CNT concentrations below 0.015%. For higher concentrations, light absorption from MWCNTs starts to play a role, resulting in the loss of transparency and loss of part of solar radiation available for current generation.

The photoanodes were dye sensitized by immersion in a 0.5 mM ethanolic solution of the commercial N719 dye (Ruthenizer 535-bisTBA from Solaronix) for 24 h. Solar cells were assembled using a standard platinized counter electrode, 25 μm thick spacer, and the iodine redox couple as electrolyte.

Figure 1a,b,d–f displays SEM images of samples prepared with the highest MWCNT concentration. It was not possible to obtain SEM images of MWCNTs from any other sample due to very low MWCNT concentration and complete coverage of MWCNTs by TiO_2 nanoparticles. The surface of the film presents deep cracks propagating through the entire film thickness (Figure 1b), which are not present in the samples with lower MWCNT concentration, whose surface appears as in the white rectangle, completely crack-free. The comparison with bare TiO_2 (Figure 1c) indicates that MWCNTs induce the formation of holes in the microstructure of TiO_2 (Figure 1d). High-resolution SEM (Figure 1e,f) clearly shows the presence of MWCNT bundles and the conformal coverage of MWCNTs by titania nanoparticles, which prevents MWCNTs from being directly imaged in samples with low MWNCT concentration.

X-ray diffraction (XRD) patterns and Raman spectra of MWCNT–TiO_2 films are shown in Figure 1g,h, respectively. XRD analysis reveals reflections only from the pure anatase phase, according to previous literature on similar systems,[13,30] without any contribution from MWCNTs, since the MWCNT concentration is below XRD detection limit. In Raman spectra, instead, the D and G bands of MWCNTs at about 1350 and 1582 cm^{-1}, which can be attributed to MWCNT defects, a disorder-induced mode, and in-plane E_{2g} zone-center mode, are clearly visible even at low MWCNT concentrations (0.010%).[13] This result further confirms the presence of MWCNTs in the nanocomposite even at low MWCNT concentration, as the tubes preserve their original structure after the high temperature annealing of the film.

The current density versus applied voltage curves in dark and under AM 1.5 G irradiation (100 mW cm^{-2}) are shown in

dx.doi.org/10.1021/jp403553t | J. Phys. Chem. C 2013, 117, 14510–14517

Figure 2, while the corresponding device parameters are reported in Table 1. The cell with the best performance is

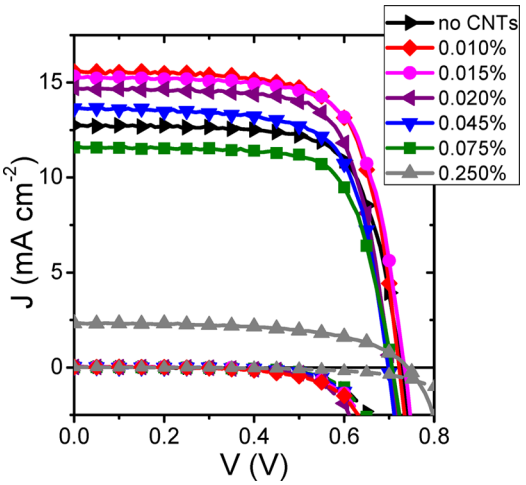

Figure 2. Current density−voltage curves of solar cells fabricated using films with different CNT content (solid lines, AM1.5G irradiation (100 mW cm^{-2}); dashed lines, dark).

obtained in the case of MWCNT−TiO_2 (0.010% wt.) films and is characterized by PCE as high as 8.1%, which represents an approximate 25% increase with respect to the layer without MWCNTs (6.5%).

In addition, we analyzed the dependence of the main photovoltaic parameters (i.e., J_{sc}, the open circuit voltage (V_{oc}), *FF*, and PCE) from both the thickness of the photoanodes (see Figure S4, Supporting Information and comments therein) as well as MWCNTs content.

The insertion of increasing percentages of MWCNTs inside the TiO_2 network (Figure S5, Supporting Information) results in a slightly enhanced dye loading for samples in the range of 0.010−0.020% MWCNTs, while the average number of N719 mols per volume unit is increased more than three times in the sample with 0.25% MWCNTs with respect to pure titania (see Supporting Information, Figure S3). This latter finding is to be considered detrimental for cell performance: it is well recognized that the optimal PCE can be obtained when the dye is chemisorbed in a closely packed monolayer, whereas the chemisorption of multilayers jeopardizes the overall performance.[31] We investigated the influence of kinetics of dye uptake in the sample with the highest MWCNT concentration, to correlate the poor performance with high dye loading (see Figure S6, Supporting Information).[32] However, as can be seen in Figure S6, the low PCE is not directly related to the amount of dye, but rather to the high MWCNT concentration, according to the hypothesis that excess in MWCNTs negatively affects the properties of charge collection of the composite network.

Anchoring of dye N719 to the photoanode surface was investigated by infrared spectroscopy. Figure 3a displays the comparison of the diffuse reflectance Fourier transform infrared (DRIFT) spectra of two sensitized photoanodes (TiO_2 and hybrid with MWCNTs). We observed no significant differences between pristine and hybrid photoanodes, thus confirming the anchoring of dye N719 in the known way (chelation exerted by the carboxylic groups present on the molecule); however, the O−H stretching region appears changed. The wide vibrational band corresponding to the stretching mode of hydroxyl groups

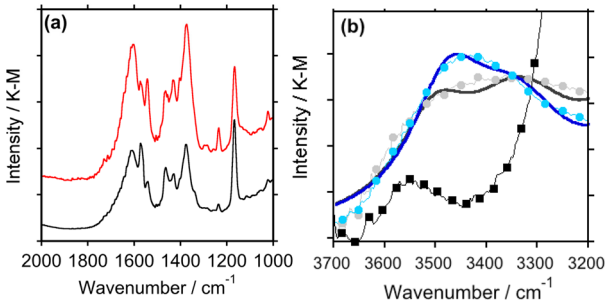

Figure 3. (a) DRIFT spectra of dye-sensitized TiO_2 (black line) and hybrid MWCNTs−TiO_2 (red line) photoanodes. *Y* axis has been shifted for clarity purposes. (b) Details of O−H stretching region for dye-sensitized TiO_2 (blue line) and hybrid MWCNTs−TiO_2 (black line) photoanodes. Symbols are experimental spectra; solid lines are fitting, and squares refer to TiO_2 photoanode before dye uptake.

is larger and less sharp for the hybrid photoanode. This region has been previously scarcely analyzed to study the anchoring of N719 to the metal oxide surface since it is supposedly less relevant for understanding the chemisorption process. However, in the present case, it can provide additional and useful information; deconvolution of this band (Figure 3b) results in a double contribution for both photoanodes: an unresolved peak centered at 3456 (3488) cm^{-1} for TiO_2 (MWCNT−TiO_2) and a second band that appears as a shoulder in TiO_2 sample (3358 cm^{-1}) and as an individual peak at 3330 cm^{-1} for the hybrid structure. The relative intensity of these vibrations is inverted for the two samples, and they are due to neither the stretching of hydroxyl groups originally present on TiO_2, which is instead visible at 3555 cm^{-1}, nor to the acid free ν(O−H) of dye N719.[33] The band is due to linear (Ti−OH) and bridged (Ti−OH−Ti) hydroxyl groups, and there can be also a contribution for surface adsorbed water molecules (more likely absent in our case after the annealing treatment). According to the native position of O−H stretching in the TiO_2 sample, the band can be attributed to free O−H oscillators in simple titania, while bonded oscillators are observed in dye-sensitized samples. It is also known that the presence of these groups, as well as the ratio between them, depends on the types of exposed facets and on the presence of surface sites in the low coordination configuration.[34]

These differences highlighted for TiO_2 and hybrid MWCNT−TiO_2 photoanodes are ascribed to different O−H sites available for TiO_2 and hybrid MWCNT−TiO_2 photoanodes as binding sites for the dye. The interfacial configuration dye/metal oxide is one of the critical parameters in DSC performance, and the identified differences could account for the increase in dye loading with MWCNT concentrations.

The dependence of the device properties on MWCNTs concentration in films with optimized thickness (12.5−15 μm) is reported in Figure 4. PCE and J_{sc} reach a maximum peak at quite low concentration (0.010−0.015%); V_{oc} monotonically decreases as MWCNT concentration increases up to 0.075%, while it is significantly higher for the sample 0.250%. The *FF* is weakly affected by MWCNT content except for 0.250% concentration, for which it is significantly lower.

The device parameters of the cells can be interpreted in terms of the modified optical and electronic transport properties induced by adding MWCNTs. MWCNTs content below 0.015% has a negligible effect on film transparency (Figure S1, Supporting Information), while it enhances

dx.doi.org/10.1021/jp403553t | J. Phys. Chem. C 2013, 117, 14510−14517

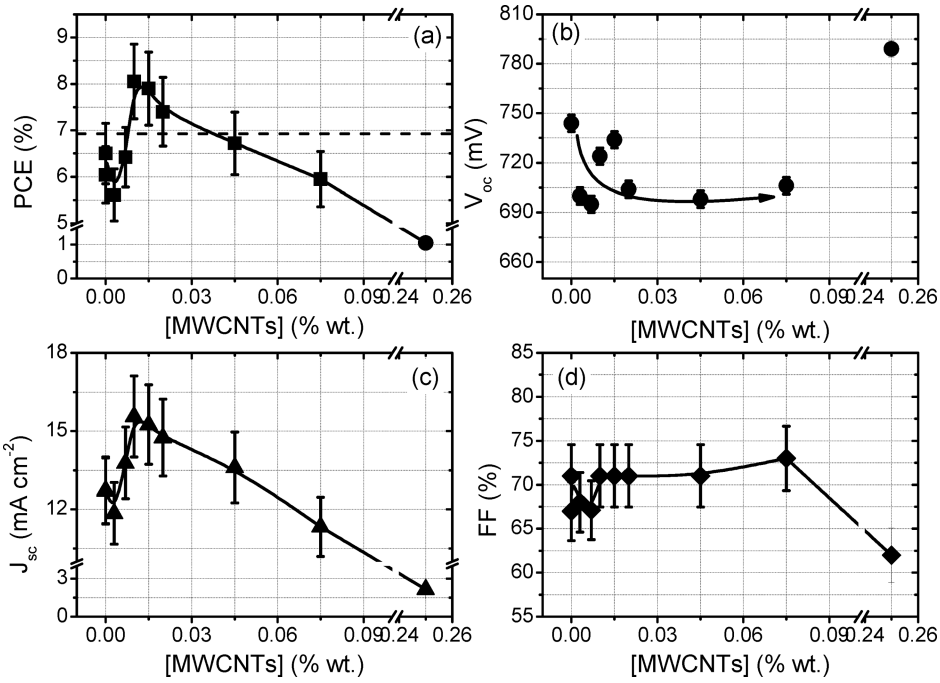

Figure 4. Functional properties of DSCs under AM1.5G irradiation (100 mW cm^{-2}) as a function of CNT concentration. (a) PCE; (b) V_{oc}; (c) J_{sc}; (d) *FF*. Photoanode thickness ranges from 9 up to 12 μm. The horizontal straight line in panel a indicates a PCE value at least 10% higher than the undoped layer. Solid lines are guides for the eye.

significantly the electron mobility of the photoanode. Such conditions represent an optimum combination to obtain light absorption exclusively from dye molecules (being light losses due to MWCNTs absorption of minor importance) and faster charge collection than in undoped samples, resulting in limited recombination (see the effect on J_{sc}) and enhanced PCE. On the contrary, in heavily doped layers, competitive light absorption from MWCNTs is significant, leading to partial loss of available radiation. However, this effect is insufficient to completely account for the strong reduction in collected charge and PCE, as also shown from the reduced *FF* in heavily doped layers.

These results are quite different with respect to the ones presented by Kamat and co-workers (in a single-walled CNT/rutile nanoparticles system):[35] in fact, in that case, the improvement in photocurrent generation was completely neutralized by a significantly lower photovoltage, without any significant increase of PCE. In ref 30, an increase in efficiency was reported for quite high MWCNTs concentrations (0.1 wt % and above), but the highest efficiency was 4.62%, which is at present below the PCE of our cell produced with bare TiO_2, so the results cannot be directly compared.

Transient photovoltage decay and electrochemical impedance spectroscopy (EIS) were applied to further elucidate the role of MWCNTs doping on the electronic properties of the photoanodes. Figure 5 reports the electron lifetime (τ_e) as obtained from transient photovoltage decay of cells with different MWCNTs contents and optimized thickness (selected samples from Table 1). A fast method to calculate directly τ_e from the transient photovoltage decay is given by[36,37] $\tau_e = (k_B T/e)(dV_{OC}/dt)^{-1}$, where k_B is the Boltzmann constant, T is the absolute temperature, and e is the elementary charge. τ_e is intimately related to the nature of the interface oxide/dye/electrolyte and the recombination phenomena that affect charge transport during cell operation.

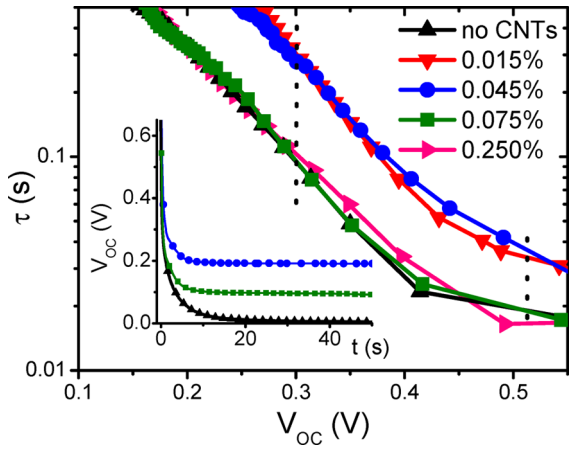

Figure 5. Electron lifetime obtained from V_{oc} decay measurements. Inset: V_{oc} decay for three different cells (black, 0% CNTs; blue, 0.045 wt % CNTs; green, 0.075 wt % CNTs).

For voltages higher than 200 mV, the curves can be grouped in two different families: the first one is represented by the moderately doped samples (0.010−0.045%), the second one comprises the undoped layer and the photoanodes with MWCNTs content larger than 0.015%. Moderate MWCNT addition results in longer electron lifetime (0.30 s at 300 mV and 0.04 s at 500 mV), as compared to undoped or heavily doped cells (0.1 and 0.02 s at the same V_{oc}, respectively). Since electron collection is directly related to electron lifetime, the experimental evidence clearly and independently confirms the previously described trends on PCE and the other device parameters. However, and rather surprisingly, elevated MWCNTs concentrations result in a reduced τ_e. A possible reason could be that at concentrations of MWCNTs above 0.25% they form random and large bundles that loop inside the TiO_2 matrix, thus acting as trapping sites that inhibit charges

dx.doi.org/10.1021/jp403553t | J. Phys. Chem. C 2013, 117, 14510−14517

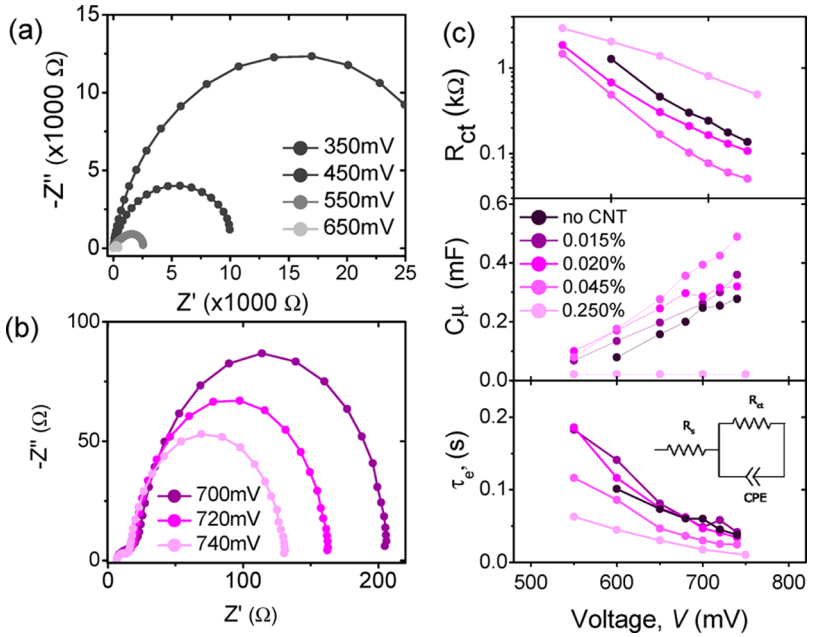

Figure 6. Electrochemical impedance spectroscopy analysis of the cell performance as a function of CNT loading. EIS spectra of one of the best performing cells in (a) low- and (b) high-bias limit. (c) (top to bottom) Charge transfer resistance R_{ct}, chemical capacitance C_μ, and electron lifetime τ_e as a function of applied biases in samples with different MWCNT loading, as labeled. These parameters were estimated by using a transmission line model (see inset in panel c, bottom, and text for details).

from fast collection at electrodes. Such poor charge collection, together with enhanced light loss due to CNT direct absorption, strongly reduces PCE with respect to all the other samples, including pristine ones. These findings are further supported by independent EIS measurements, reported in Figure 6. The slight decrease in V_{oc} at increasing MWCNT concentrations could be caused by the downshift of the potential band edge of the TiO_2 conduction band, yet is of minor importance in reducing the photoconversion efficiency of the solar cells.

Figure 6 shows a representative EIS measurement performed in dark as a function of different applied voltages for one of the highest efficiency cell (PCE = 7.9% for 0.015% MWCNT loading). Panel a refers to low biases, while panel b refers to higher biases (close to V_{oc}). All other investigated cells with different CNT loading exhibit identical features.

In the limit of high biases, we observed two characteristic arches in the EIS spectra:[36,38] the first one at high frequency, which usually accounts for the FTO/TiO_2 interface and the second in the mid-frequency range. The latter provides useful insights about the charge transfer mechanisms taking place at the interface between the TiO_2 and the electrolyte.

To retrieve the recombination and transport properties, we fitted the spectra in the mid-frequency range with the aid of the equivalent circuit of the transmission model. The model includes a series resistance (R_s) followed by the parallel of the charge transfer resistance (R_{ct}) and a CPE element (often used in lieu of a capacitor to compensate for nonhomogeneity in the system).

The product of the charge-transfer resistance and the chemical capacitance allows to estimate the electron lifetime $\tau_e = R_{ct}C_\mu$ at each applied bias. Figure 6c shows the dependence of R_{ct}, C_μ, and τ_n as a function of different biases in samples with different MWCNT loading. The reported data refer to the best performance cells with similar thickness for each CNT loading.

With R_{ct} (C_μ) decreasing (increasing) with increasing applied biases at fixed and lower concentration (top and center panel in Figure 6c), we found that the lifetime (bottom panel) decreases as a function of the applied bias by almost an order of magnitude. For large MWCNT loading (i.e., 0.250%), we observed a much smoother decrease of the R_{ct} along with an almost unaffected change in the chemical capacitance, resulting in an overall shorter electron lifetime of the order of a few tens of milliseconds.

As in the case of the study of the functional properties previously presented, EIS measurements confirm that an elevated concentration of CNTs drastically reduces the lifetime of electrons in the TiO_2 layer; this is also confirmed by the very low efficiency obtained in this case (PCE = 1.1%). These data strongly indicate that, while lower concentrations (<0.045%) of MWCNTs in the TiO_2 matrix have the overall effect of favoring the electron conduction and inhibiting the recombination process, elevated concentrations actually inhibit and/or screen charge transport toward the photoanode, according to the schematic view proposed on the basis of previously discussed optical and device properties.

After the systematic analysis of the influence of CNT concentration and photoanode thickness on DSCs device properties, we chose the best performing material (0.010% concentration) to be studied in an optimized DSC configuration, including (i) a reflecting layer composed of large TiO_2 particles (150−250 nm in size) and (ii) increased annealing temperature up to 500 °C, which guarantees improved sintering properties of the final photoanode. The device characteristics of these optimized cells are reported in Figure S7, Supporting Information, and Table 1. The higher annealing temperature and the presence of the reflecting layer significantly enhance the properties of the MWCNT loaded cell: photoconversion efficiency increases from 7.0% in bare TiO_2 cell up to 9.0% in the 0.010%-loaded cell (maximum power density output of the best cell: 9.0 mW cm^{-2}). The analysis of the transient

dx.doi.org/10.1021/jp403553t | J. Phys. Chem. C 2013, 117, 14510−14517

photovoltage decay and of the corresponding electron lifetime (Figure S7b, Supporting Information) clearly demonstrates the beneficial effect of the enhancement of the annealing temperature on cell properties. Both the pristine and MWCNT−TiO_2 DSCs annealed at 500 °C exhibit electron lifetimes systematically higher than cells annealed at 450 °C, as can be deduced by the shift at higher V_{oc} of the solid lines in Figure S7b, Supporting Information. Such behavior is most likely due to the improved sintering of nanoparticles at higher annealing temperature, while the reflecting layer does not play a significant role from the viewpoint of the electron transport behavior of the photoanode, but acts as a light scattering barrier enhancing light capture by the active layer. In this manner, the simultaneous effect of improved light capture and electron collection is maximized, resulting in an 11% increase of PCE, up to 9.0%.

CONCLUSIONS

In conclusion, we demonstrated that a small amount of MWCNTs rapidly dispersed in a commercial TiO_2 anatase paste is able to significantly increase the photoconversion efficiency in DSCs, while also improving other device parameters. Optimized concentrations (0.010−0.020%) of MWCNTs do not affect the optical properties of the TiO_2 layer, while significantly enhancing charge collection at the photoanode. The enhancement of electron lifetime and the reduction of recombination phenomena lead to an increased photoconversion efficiency of the operating cell, with a maximum value of 9.0% in the best performance device (corresponding to the addition of 0.010 wt % MWCNTs). Hence, we demonstrated a fast, cheap, and highly effective way to increase the photoconversion efficiency in DSCs specifically, but also in generic excitonic solar cells based on polycrystalline photoanodes. Our work points to the possibility to significantly enhance the PCE in DSCs through a fast, cheap, scalable, and highly reproducible approach.

ASSOCIATED CONTENT

Supporting Information

Information about UV−vis absorbance, reproducibility in the fabrication and testing of DSSCs, dependence of functional properties of DSSCs on photoanode thickness, dye loading versus CNT content, current density versus voltage, and electron lifetime of solar cells fabricated with photoanodes annealed at 500 °C. This material is available free of charge via the Internet at http://pubs.acs.org.

AUTHOR INFORMATION

Corresponding Author

*E-mail: alberto.vomiero@ing.unibs.it (A.V.); isabella.concina@ing.unibs.it (I.C.); rosei@emt.inrs.ca (F.R.).

Author Contributions

¶K.T.D. and G.S.S. contributed equally to this work.

Notes

The authors declare no competing financial interest.

ACKNOWLEDGMENTS

The European Commission under the Project WIROX (contract no. 295216, FP7-PEOPLE-2011-IRSES), OIKOS s.r.l. (Brescia), and MDEIE (Quebec) are acknowledged for partial funding of this project. F.R. is grateful to the Canada Research Chairs program for partial salary support and to the FRQNT team grants program. A.V. acknowledges the European Commission for partial funding under the Project F-LIGHT (contract no. 299490, FP7-PEOPLE-2011-IOF). C.S. and I.C. acknowledge financial support from Region Lombardia (Italy) under "Dote Ricercatore" fellowship and X-Nano project "Emettitori di elettroni a base di nano tubi di carbonio e nano strutture di ossidi metallici quasi monodimensionale per lo sviluppo di sorgenti a raggi X", respectively. J.C.R. acknowledges the International Centre for Theoretical Physics (ICTP) for partial funding under the TRIL programme.

REFERENCES

(1) O'Regan, B.; Graetzel, M. A Low-Cost, High-Efficiecy Solar Cell Based on Dye-Sensitized Colloidal TiO_2 Films. *Nature* **1991**, *353*, 737−740.

(2) Graetzel, M. Photoelectrochemical Cells. *Nature* **2001**, *414*, 338−344.

(3) Vomiero, A.; Concina, I.; Comini, E.; Soldano, C.; Ferroni, M.; Faglia, G.; Sberveglieri, G. One-Dimensional Nanostructured Oxides for Thermoelectric Applications and Excitonic Solar Cells. *Nano Energy* **2012**, *1*, 372−390.

(4) Galstyan, V.; Vomiero, A.; Concina, I.; Braga, A.; Brisotto, M.; Bontempi, E.; Faglia, G.; Sberveglieri, G. Vertically Aligned TiO_2 Nanotubes on Plastic Substrates for Flexible Solar Cells. *Small* **2011**, *7*, 2437−2442.

(5) Varghese, O. K.; Paulose, M.; Grimes, C. A. Long Vertically Aligned Titania Nanotubes on Transparent Conducting Oxide for Highly Efficient Solar Cells. *Nat. Nanotechnol.* **2009**, *4*, 592−597.

(6) Law, M.; Greene, L. E.; Johnson, J. C.; Saykally, R.; Yang, P. D. Nanowire Dye-Sensitized Solar Cells. *Nat. Mater.* **2005**, *4*, 455−459.

(7) Baxter, J. B.; Aydil, E. S. Nanowire-Based Dye-Sensitized Solar Cells. *Appl. Phys. Lett.* **2005**, *86*, 053114.

(8) Vomiero, A.; Concina, I.; Natile, M. M.; Comini, E.; Faglia, G.; Ferroni, M.; Kholmanov, I.; Sberveglieri, G. ZnO/TiO_2 Nanonetwork as Efficient Photoanode in Excitonic Solar Cells. *Appl. Phys. Lett.* **2009**, *95*, 193104.

(9) Tan, B.; Wu, Y. Dye-Sensitized Solar Cells Based on Anatase TiO_2 Nanoparticle/Nanowire Composites. *J. Phys. Chem. B* **2006**, *110*, 15932−15938.

(10) Memarian, N.; Concina, I.; Braga, A.; Rozati, S. M.; Vomiero, A.; Sberveglieri, G. Hierarchically Assembled ZnO Nanocrystallites for High-Efficiency Dye-Sensitized Solar Cells. *Angew. Chem., Int. Ed.* **2011**, *50*, 12321−12325.

(11) Zhang, Q.; Chou, T. P.; Russo, B.; Jenekhe, S. A.; Cao, G. Aggregation of ZnO Nanocrystallites for High Conversion Efficiency in Dye-Sensitized Solar Cells. *Angew. Chem., Int. Ed.* **2008**, *47*, 2402−2406.

(12) Kongkanand, A.; Martínez Domínguez, R.; Kamat, P. V. Single Wall Carbon Nanotube Scaffolds for Photoelectrochemical Solar Cells. Capture and Transport of Photogenerated Electrons. *Nano Lett.* **2007**, *7*, 676−680.

(13) Chan, Y.-F.; Wang, C.-C.; Chen, B.-H.; Chen, C.-Y. Dye-Sensitized TiO_2 Solar Cells Based on Nanocomposite Photoanode Containing Plasma-Modified Multi-Walled Carbon Nanotubes. *Prog. Photovoltaics* **2013**, *21*, 47−57.

(14) Sawatsuk, T.; Chindaduang, A.; Sae-Kung, C.; Pratontep, S.; Tumcharern, G. Dye-Sensitized Solar Cells Based on TiO_2−MWCNTs Composite Electrodes: Performance Improvement and Their Mechanisms. *Diamond Relat. Mater.* **2009**, *18*, 524−527.

(15) Dresselhaus, M. S.; Dresselhaus, G.; Avouris, P. *Carbon Nanotubes: Synthesis, Structure, Properties and Applications*; Springer-Verlag: Berlin, Germany, 2001.

(16) Martel, R.; Schmidt, T.; Shea, H. R.; Hertel, T.; Avouris, P. Single- and Multi-Wall Carbon Nanotube Field-Effect Transistors. *Appl. Phys. Lett.* **1998**, *73*, 2447−2449.

(17) Gayathri, V.; Geetha, R. Carbon Nanotube as Nems Sensor: Effect of Chirality and Stone-Wales Defect Intend. *J. Phys.: Conf. Ser.* **2006**, *34*, 824−828.

(18) Modi, A.; Kotoktar, N.; Lass, E.; Wei, B.; Ajayan, P. M. Miniaturized Gas Ionization Sensors Using Carbon Nanotubes. *Nature* **2003**, *424*, 171−174.
(19) An, K. H.; Jeon, K. K.; Heo, J. K.; Lim, S. C.; Bae, D. J.; Leez, Y. H. High-Capacitance Supercapacitor Using a Nanocomposite Electrode of Single-Walled Carbon Nanotube and Polypyrrole. *J. Electrochem. Soc.* **2002**, *149*, A1058−A1062.
(20) Pushparaj, V. L.; Shaijumon, M. M.; Kumar, A.; Marugesan, S.; Ci, L.; Vajtai, R.; Linhardt, R. J.; Nalamasu, O.; Ajayan, P. M. Flexible Energy Storage Devices Based on Nanocomposite Paper. *Proc. Natl. Acad. Sci. U.S.A.* **2007**, *104*, 13574−13577.
(21) Das, S.; Sudhagar, P.; Verma, V.; Song, D.; Ito, E.; Lee, S. Y.; Kang, Y. S.; Choi, W. B. Amplifying Charge-Transfer Characteristics of Graphene for Triiodide Reduction in Dye-Sensitized Solar Cells. *Adv. Funct. Mater.* **2011**, *21*, 3729−3736.
(22) Wang, X.; Zhi, L.; Tsao, N.; Tomovic, Z.; Li, J.; Muellen, K. Transparent Carbon Films as Electrodes in Organic Solar Cells. *Angew. Chem., Int. Ed.* **2008**, *47*, 2990−2992.
(23) Zhang, D. W.; Li, X. D.; Li, H. B.; Chen, S.; Sun, Z.; Yin, X. J.; Huang, S. M. Graphene-Based Counter Electrode for Dye-Sensitized Solar Cells. *Carbon* **2011**, *49*, 5382−5388.
(24) Hasobe, T.; Fukuzumi, S.; Kamat, P. V. Organized Assemblies of Single Wall Carbon Nanotubes and Porphyrin for Photochemical Solar Cells: Charge Injection from Excited Porphyrin into Single-Walled Carbon Nanotubes. *J. Phys. Chem. B* **2006**, *110*, 25477−25484.
(25) Lee, T. Y.; Alegaonkar, P. S.; Yoo, J.-B. Fabrication of Dye Sensitized Solar Cell Using TiO_2 Coated Carbon Nanotubes. *Thin Solid Films* **2007**, *515*, 5131−5135.
(26) Lee, K.-M.; Hu, C.-W.; Chen, H.-W.; Ho, K.-C. Incorporating Carbon Nanotube in a Low-Temperature Fabrication Process for Dye-Sensitized TiO_2 Solar Cells. *Sol. Energy Mater. Sol. Cells* **2008**, *92*, 1628−1633.
(27) Dembele, K. T.; Nechache, R.; Vomiero, A.; Santato, C.; Nikolova, L. M.; Licoccia, S.; Rosei, F. Effect of Multi-Walled Carbon Nanotubes on the Stability of Dye Sensitized Solar Cells. *J. Power Sources* **2013**, *233*, 93−97.
(28) Kubelka, P.; Munk, F. Ein Beitrag Zur Optik Der *Farbanstriche Z. Tech. Phys.* **1931**, *12*, 593−601.
(29) Kortüm, G. *Reflectance Spectroscopy*; Springer: New York, 1969.
(30) Yen, C.-Y.; Lin, Y.-F.; Liao, S.-H.; Weng, C.-C.; Huang, C.-C.; Hsiao, Y.-H.; Ma, C.-C. M.; Chang, M.-C.; Shao, H.; Tsai, M.-C.; et al. Preparation and Properties of a Carbon Nanotube-Based Nanocomposite Photoanode for Dye-Sensitized Solar Cells. *Nanotechnology* **2008**, *19*, 375305.
(31) Nelson, R. C. Energy Transfers between Sensitizer and Substrate. III. Sensitization by Thick Dye Films. *J. Opt. Soc. Am.* **1961**, *51*, 1182−1186.
(32) Concina, I.; Frison, E.; Braga, A.; Silvestrini, S.; Maggini, M.; Sberveglieri, G.; Vomiero, A.; Carofiglio, T. On-Line Monitoring and Active Control of Dye Uptake in Dye-Sensitised Solar Cells. *Chem. Commun.* **2011**, *47*, 11656−11658.
(33) Finnie, K. S.; Bartlett, J. R.; Woolfrey, J. L. Vibrational Spectroscopic Study of the Coordination of (2,2′-Bipyridyl-4,4′-dicarboxylic acid)ruthenium(II) Complexes to the Surface of Nanocrystalline Titania. *Langmuir* **1998**, *14*, 2744−2749.
(34) Minella, M.; Faga, M. G.; Maurino, V.; Minero, C.; Pelizzetti, E.; Coluccia, S.; Martra, G. Effect of Fluorination on the Surface Properties of Titania P25 Powder: An FTIR Study. *Langmuir* **2010**, *26*, 2521−2527.
(35) Brown, P.; Takechi, K.; Kamat, P. V. Single-Walled Carbon Nanotube Scaffolds for Dye-Sensitized Solar Cells. *J. Phys. Chem. C* **2008**, *112*, 4776−4782.
(36) Bisquert, J.; Fabregat-Santiago, F.; Mora-Sero, I.; Garcia-Belmonte, G.; Giménez, S. Electron Lifetime in Dye-Sensitized Solar Cells: Theory and Interpretation of Measurements. *J. Phys. Chem. C* **2009**, *113*, 17278−17290.
(37) Zaban, A.; Greenshtein, M.; Bisquert, J. Determination of the Electron Lifetime in Nanocrystalline Dye Solar Cells by Open-Circuit Voltage Decay Measurements. *Chem. Phys. Chem.* **2003**, *4*, 859−864.
(38) Bisquert, J. Theory of the Impedance of Electron Diffusion and Recombination in a Thin Layer. *J. Phys. Chem. B* **2002**, *106*, 325−333.